Title
Sensitivity of MJO propagation to a robust positive Indian Ocean dipole event in the superparameterized CAM

Journal
Journal of Advances in Modeling Earth Systems, 7(4)

ISSN
1942-2466

Authors
Benedict, James J
Pritchard, Michael S
Collins, William D

Publication Date
2015-12-01

DOI
10.1002/2015ms000530

Peer reviewed

AGU PUBLICATIONS

Journal of Advances in Modeling Earth Systems

RESEARCH ARTICLE
10.1002/2015MS000530

Sensitivity of MJO propagation to a robust positive Indian Ocean dipole event in the superparameterized CAM

James J. Benedict[1,2], Michael S. Pritchard[3], and William D. Collins[1,4]

[1]Department of Climate Sciences, Lawrence Berkeley National Laboratory, Berkeley, California, USA, [2]Now at Rosenstiel School of Marine and Atmospheric Science, University of Miami, Florida, USA, [3]Department of Earth System Science, University of California-Irvine, Irvine, California, USA, [4]Department of Earth and Planetary Science, University of California-Berkeley, Berkeley, California, USA

Key Points:
- Superparameterized CAM reproduces observed MJO weakening during positive Indian Ocean Dipole events
- Interannual and subseasonal circulation and moist static energy changes disrupt MJO
- MJO disruption linked to coexisting warm equatorial Pacific SSTs during positive IOD phase

Correspondence to:
J. J. Benedict,
jjbenedict@lbl.gov

Citation:
Benedict, J. J., M. S. Pritchard, and W. D. Collins (2015), Sensitivity of MJO propagation to a robust positive Indian Ocean dipole event in the superparameterized CAM, *J. Adv. Model. Earth Syst.*, *7*, 1901–1917, doi:10.1002/2015MS000530.

Received 6 AUG 2015
Accepted 29 OCT 2015
Accepted article online 31 OCT 2015
Published online 23 NOV 2015

Abstract The superparameterized Community Atmosphere Model (SPCAM) is used to investigate the impact and geographic sensitivity of positive Indian Ocean Dipole (+IOD) sea-surface temperatures (SSTs) on Madden-Julian oscillation (MJO) propagation. The goal is to clarify potentially appreciable +IOD effects on MJO dynamics detected in prior studies by using a global model with explicit convection representation. Prescribed climatological October SSTs and variants of the SST distribution from October 2006, a +IOD event, force the model. Modest MJO convection weakening over the Maritime Continent occurs when either climatological SSTs, or +IOD SST anomalies restricted to the Indian Ocean, are applied. However, severe MJO weakening occurs when either +IOD SST anomalies are applied globally or restricted to the equatorial Pacific. MJO disruption is associated with time-mean changes in the zonal wind profile and lower moist static energy (MSE) in subsiding air masses imported from the Subtropics by Rossby-like gyres. On intraseasonal scales, MJO disruption arises from significantly smaller MSE accumulation, weaker meridional advective moistening, and overactive submonthly eddies that mix drier subtropical air into the path of MJO convection. These results (1) demonstrate that SPCAM reproduces observed time-mean and intraseasonal changes during +IOD episodes, (2) reaffirm the role that submonthly eddies play in MJO propagation and show that such multiscale interactions are sensitive to interannual SST states, and (3) suggest that boreal fall +IOD SSTs local to the Indian Ocean have a significantly smaller impact on Maritime Continent MJO propagation compared to contemporaneous Pacific SST anomalies which, for October 2006, resemble El Niño-like conditions.

1. Introduction

It is well known that the Madden-Julian oscillation (MJO) can be sensitive to slowly varying sea-surface temperature (SST) patterns such as those forced by large-scale seasonal [*Salby and Hendon*, 1994; *Zhang and Dong*, 2004] and interannual (ENSO) effects [*Fink and Speth*, 1997; *Kessler and Kleeman*, 2000; *Zhang and Gottschalck*, 2002]. In contrast, the impact of smaller-scale, subbasin background variations in SST in the MJO's genesis region is less clear. The Indian Ocean Dipole (IOD) [*Saji et al*., 1999] modulates SSTs, low-level winds, precipitation, and upper-ocean dynamics in a regional pattern, sometimes independently of signals from the Pacific Ocean [*Reverdin et al*., 1986; *Webster et al*., 1999; *Saji et al*., 1999; *Cai et al*., 2014]. Low-frequency (seasonal to interannual) IOD activity is significantly correlated with high-frequency (subseasonal) variability such as the MJO [*Shinoda and Han*, 2005; *Sooraj et al*., 2009; *Kug et al*., 2009], but our understanding of the detailed mechanisms involved in this relationship is limited.

Improved understanding of the IOD-MJO nexus could help inform modern MJO theory and field campaign measurement deployments. MJO weakening has been noted in observations during the +IOD phase [*Wilson et al*., 2013] associated with reduced climatological low-level zonal westerlies [*Inness et al*., 2003; *Zhang et al*., 2006]. It is logical to expect that this could impede theorized MJO moisture advection dynamics [*Maloney*, 2009; *Sobel and Maloney*, 2013] or, through associated reduced easterly vertical shear, impede theorized MJO equatorial wave dynamics [*Wang and Xie*, 1996; *Sooraj et al*., 2009]. These dynamics are in debate yet may be relevant to understanding the 2006 Mirai Indian Ocean cruise for the Study of the Madden-Julian oscillation (MJO)-convection Onset (MISMO) [*Yoneyama et al*., 2008], in which suppressed MJO eastward propagation has been attributed to an amplified +IOD state [*Yoneyama et al*., 2008; *Horii et al*., 2008].

Improved understanding of the +IOD phase impact on the MJO is also critical for tropical climate change dynamics. Projections from the Coupled Model Intercomparison Project phase 5 [*Taylor et al*., 2012] suggest the frequency of extreme +IOD events will increase by a factor of three by the end of the 21st century [*Cai et al*., 2013b,2014]. Thus, if a robust +IOD MJO disruption effect exists, it could importantly counteract the striking thermodynamic amplification of the MJO seen in, e.g., *Jones and Carvalho* [2011] and *Arnold et al*. [2013, 2015]. *Maloney and Xie* [2013] point out that the MJO as simulated in their model can be highly sensitive to the spatial pattern of SST warming.

Motivated by the above, our strategy is to determine the impact of a perturbed +IOD SST forcing on the MJO in the superparameterized Community Atmosphere Model (hereafter, "SPCAM") [*Khairoutdinov and Randall*, 2001; *Khairoutdinov et al*., 2008], a global climate model capable of producing realistic MJO disturbances [*Benedict and Randall*, 2009] while making minimal assumptions about moist convection [*Grabowski and Smolarkiewicz*, 1999; *Khairoutdinov and Randall*, 2003]. A secondary motivation is to discriminate the local Indian Ocean SST dipole effects from remote tropical Pacific SST anomalies that can also associate with the +IOD phase. This is relevant to an ongoing debate about the dependence [*Dommenget*, 2011; *Zhao and Nigam*, 2015] or independence [*Saji and Yamagata*, 2003; *Fischer et al*., 2005; *Meyers et al*., 2007] between the IOD and ENSO. This study is not aimed at fully disentangling the potential IOD-ENSO link; however, we do demonstrate sensitivities in the simulated MJO response to perturbed SST conditions in different geographic sectors referenced from a single but representative +IOD event.

The SPCAM experiment design and MJO compositing method are described in section 2. Results from these simulations are presented in section 3. Section 4 provides an interpretation of the results and a summary of the key findings.

2. Data, Model Setup, and Methods

Observed SST data, described in *Hurrell et al*. [2008] and currently available from https://climatedataguide.ucar.edu/climate-data/merged-hadley-noaaoi-sea-surface-temperature-sea-ice-concentration-hurrell-et-al-2008, are used to identify IOD events and provide lower boundary forcing in our SPCAM simulations. The gridded monthly data are optimized for use in CAM simulations and are bilinearly interpolated from their native $1^\circ \times 1^\circ$ resolution to the model's T42 (2.8°) grid.

IOD amplitudes during the period January 1965 to March 20012 are quantified using the Dipole Mode Index (DMI) [*Saji et al*., 1999] and follow the methods of *Saji and Yamagata* [2003]. SST anomalies are computed by removing the climatological mean for each month, removing the long-term linear trend, removing low-frequency oscillatory signals with periods greater than 7 years, and removing intraseasonal signals by applying a 3 month running average. The results are area-averaged over the west Indian Ocean (WIO; $50^\circ - 70^\circ$E, 10°S-10°N) and east Indian Ocean (EIO; $90^\circ - 110^\circ$E, 10°S-0°S). The DMI is computed by standardizing the WIO–EIO difference. Because the IOD is seasonally phase locked with peak amplitude in the boreal fall [*Saji et al*., 1999], we identify Octobers with DMI $\geq 1\sigma$ as +IOD events. Because a 3 month running average has been applied to the SST data, the October DMI will contain some information from September and November. Unlike in *Saji and Yamagata* [2003], the time-lagged ENSO-driven Indian Ocean basin-average SST response is not removed from the data here. This should not strongly influence identification of October IOD events because the Indian Ocean basin-wide SST response occurs at least 4–5 months following the peak of ENSO events [*Klein et al*., 1999; *Saji and Yamagata*, 2003], which typically reach a maximum amplitude in the boreal winter [*Harrison and Larkin*, 1998]. A weak +IOD-like pattern in Indian Ocean SSTs during the October preceding the peak amplitude of a composite ENSO event is noted in *Okumura and Deser* [2010], however. A more rigorous accounting of direct ENSO influences would likely reduce the magnitude of +IOD SST anomalies used in the present study.

A total of 8 October +IOD events were identified within the 1965–2012 period (1972, 1982, 1987, 1991, 1994, 1997, 2002, and 2006). With the exception of 1991 and 1994, the remaining +IOD events had contemporaneous Niño3.4 indices [*Trenberth*, 1997] greater than $+1\sigma$ supporting the known ENSO influence on Indian Ocean SSTs [see *Schott et al*., 2009 review]. Recent analysis by *Zhao and Nigam* [2015] indicates that the IOD is manifested more clearly in upper ocean heat content rather than SST. Those authors find that the +IOD events of 1994 and 2006 exhibit clear dipole variability in subsurface ocean temperatures even when ENSO influences are removed, suggesting that these two events are manifested largely by processes

internal to the Indian Ocean region and are representative of the canonical +IOD. For this reason and for the motivating factors mentioned in section 1, SST anomaly distributions from October 2006 are selected as perturbed lower boundary forcings for our SPCAM simulations.

The numerical model is the superparameterized CAM version 3.0 configured as in *Pritchard and Bretherton* [2014] with an exterior/interior horizontal resolution of T42/4km and a vertical grid of 30 levels, consistent with the most widely scrutinized configuration of SPCAM3 that produces realistic MJO signals [*Khairoutdinov et al*., 2008; *Benedict and Randall*, 2009]. For computational efficiency, the interior cloud resolving models (CRM) are shrunk from the standard 128 km extent to 32 km extent, but this is not expected to impact the simulated MJO given its intrinsic insensitivity to CRM extent documented in *Pritchard et al*. [2014].

Four 15 year SPCAM simulations are examined in this study. All runs use identical configurations and external boundary conditions except for the distribution of prescribed SST. CLIM is a control simulation forced by observed 1965–2012 October mean SSTs and sea ice concentrations. Three variants of the October 2006 SST pattern (a +IOD event concurrent with a moderate warm ENSO signal) are also examined. In 2006Glb, October 2006 SST anomalies are added to the climatological October mean for all global grid points. Cases 2006IO and 2006Pac are similar to 2006Glb except that SST anomalies are only applied in the equatorial Indian and Pacific Oceans, respectively (see Figure 1). A weighting function restricting SST anomalies to either the equatorial (20°S−20°N) Indian (40°−120°E) or Pacific (150°E−90°W) regions is linearly tapered from 1 (within selected domain) to 0 (outside of selected domain) over a 20° wide (30° wide) buffer zone in latitude (longitude).

MJO identification and tracking techniques of *Ling et al*. [2013] and *Ling et al*. [2014] are used to construct MJO lag composites. Intraseasonal convective episodes are identified when area-averaged (60°−90°E, 7°S−15°N) precipitation anomalies, defined as perturbations from a smoothed calendar-day mean that are linearly detrended and smoothed with a 7 day low-pass filter, exceed $+1\sigma$ for at least 3 consecutive days. The first of the consecutive string of days is labeled "Day-0." Evaluation of eastward propagation is determined by examining 7°S−15°N-averaged precipitation anomalies $\bar{P}$: if (1) Day-0 $\bar{P}$ at any longitude within (60°−90°E) exceeds $+1\sigma$ (where σ is the average standard deviation of $\bar{P}$ between 60°−120°E) and (2) $\bar{P}$ at 100°E subsequently exceeds $+1\sigma$ between 0 and 15 days following MJO initiation (Day-0), the intraseasonal disturbance is considered an eastward-propagating event. A representative propagation speed for each disturbance is computed following *Ling et al*. [2014]: a series of straight lines spanning (40°E−160°W) is applied to a Hovmöller diagram of $\bar{P}$, with each line originating at Day 0 along the chosen western boundary but with incrementally varying slopes associated with propagation speeds from 3 to 13 m s^{-1}. The slope corresponding to $\bar{P}_{max}$, the maximum along-line sum of positive $\bar{P}$, defines the propagation speed of each event. The 10% weakest-amplitude MJO disturbances, as defined by $\bar{P}_{max}$, are discarded. Variations of this MJO identification and tracking technique have been successfully used in several recent studies [*Subramanian and Zhang*, 2014; *Ulate et al*., 2015].

3. Results

3.1. Connection Between MJO and SST Distribution

The geographic SST distributions and resulting MJO precipitation anomaly propagation for each SPCAM simulation are shown in Figure 1. Unless noted otherwise, here and for the remainder of this paper, anomalies are defined as perturbations from a smoothed calendar-day mean that are linearly detrended and smoothed with a 7 day low-pass filter. During October, the warmest SSTs (Figure 1a), heaviest mean precipitation, and largest MJO variability (not shown) occur between 7°S and 15°N, motivating the selected latitude range for MJO lag composites. Our conclusions are not sensitive to moderate adjustments of this latitude range. Although CLIM October SST forcing spans 1965–2012, its time-mean tropical precipitation generally compares favorably to 1981–2010 October mean rainfall from the Global Precipitation Climatology Project (GPCP) [*Adler et al*., 2003] with the exception of positive rainfall biases up to a factor of 1.5–2.0 in the central Indian and west Pacific Oceans (not shown). The simulated rainfall anomalies of 2006Glb are qualitatively consistent with GPCP satellite-estimated rainfall anomalies from October 2006 (not shown), with strong negative anomalies from the equatorial eastern Indian Ocean to the far west Pacific Ocean bookended by positive rainfall anomalies to the west and east.

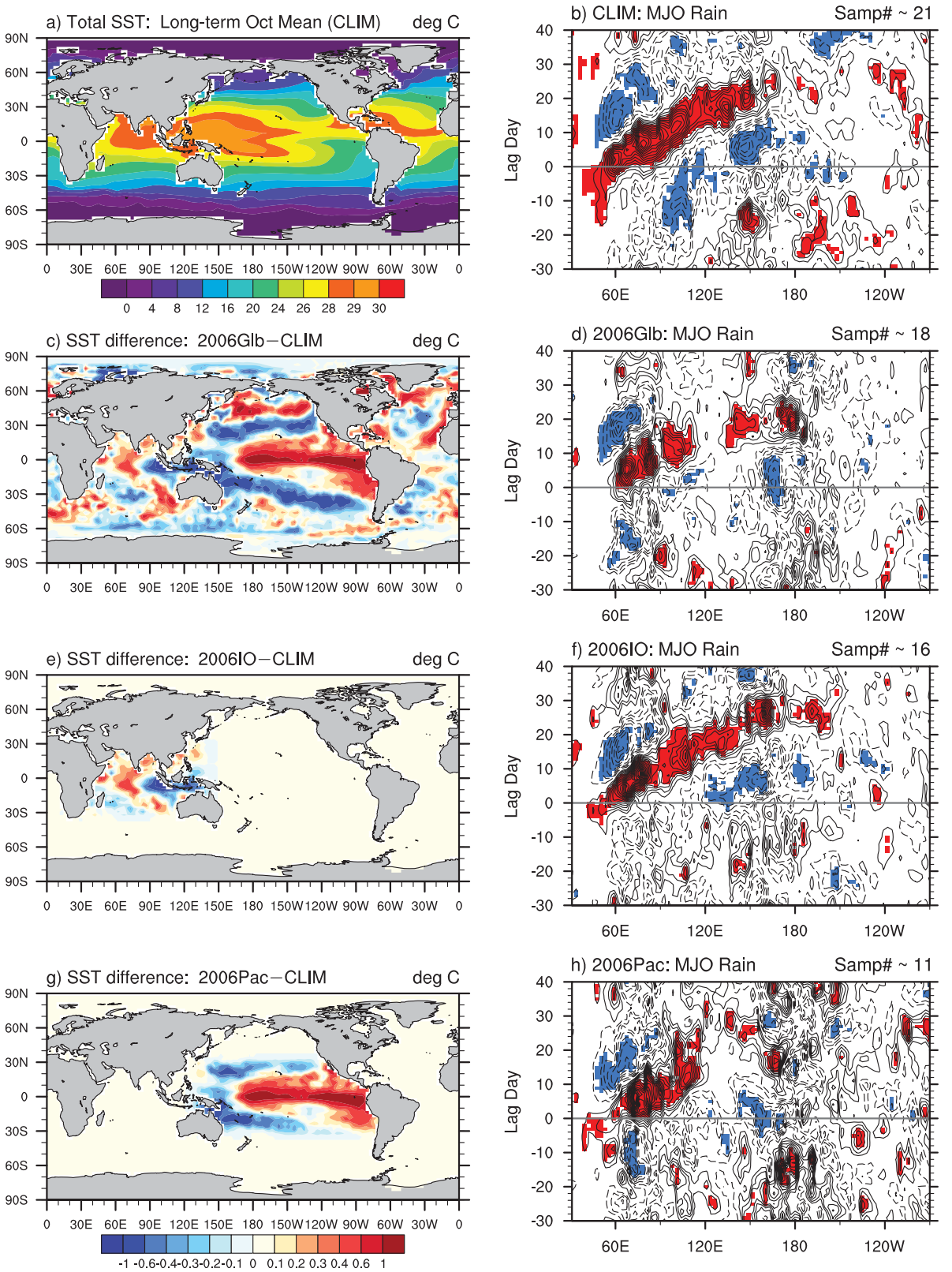

Figure 1. (left column) (a) Observed October climatological SST used to force CLIM and (c, e, g) SST differences between each experimental simulation and CLIM. (right column) Lag composite precipitation anomalies for (b) CLIM, (d) 2006Glb, (f) 2006IO, and (h) 2006Pac. Data have been averaged from 7°S to 15°N. Contour interval is 0.5 mm/d, positive (negative) anomalies are solid (dashed), and no zero contour is drawn. Positive and negative anomalies exceeding the 95% statistical significance threshold are shaded red and blue, respectively. Negative lag days occur before MJO convective initiation. Composite sample size is shown in the top right of each right-column plot.

The October 2006 global SST anomaly pattern (Figure 1c) indicates the expected negative SST gradient from west to east across the Indian Ocean associated with a +IOD event. By several metrics, the 2006 +IOD event was one of the strongest in the 1965–2012 period [*Werner et al*., 2012; *Wilson et al*., 2013]. Coexisting SST anomalies resembling El Niño occur in the equatorial Pacific Ocean [*Harrison and Larkin*, 1998; *Okumura and Deser*, 2010]. For the 2006IO and 2006Pac simulations, the October 2006 SST anomalies are confined to the equatorial Indian and Pacific Oceans, respectively (Figures 1e and 1g).

Corresponding lag composites of precipitation anomalies appear in Figure 1 (right column). As expected, the MJO identification algorithm effectively isolates MJO signals, as evidenced in CLIM (Figure 1b): deep convection forms in the western Indian Ocean and propagates eastward at a fairly constant ~5.5 m s^{-1} across the Maritime Continent and into the central Pacific where it dissipates. The coherent, robust pattern of positive rainfall anomalies (red shading) is preceded and followed by statistically significant dry anomalies (blue shading). Moderate weakening of the simulated MJO convective signal is noted between 110° and 130°E in accordance with observed propagation behavior [e.g., *Zhang and Hendon*, 1997].

Reassuringly, a realistic MJO disruption response occurs in SPCAM as a result of +IOD SST anomalies. Compared to CLIM, the MJO signal in 2006Glb (Figure 1d) weakens substantially over the Maritime Continent and propagates at an increased speed over the West Pacific, consistent with the observational results of *Wilson et al*. [2013]. The increased MJO propagation speed in 2006Glb is associated with comparatively larger tropospheric static stability (not shown) and likely reflects reduced convective coupling [e.g., *Bony and Emanuel*, 2005]. Dry anomalies, particularly leading MJO deep convection, are also weaker and less spatially coherent in 2006Glb. This IOD-induced disruption of the MJO tends to reaffirm the use of SPCAM as a tool to study IOD-MJO interactions.

The question naturally arises as to whether the MJO disruption occurs due to processes local to the Indian Ocean, or associated SST anomalies elsewhere. Figure 1 shows that when +IOD SST anomalies are restricted to the equatorial Indian Ocean (2006IO, Figure 1e), the MJO signal is weakened over the Maritime Continent but not nearly to the extent seen in 2006Glb. That is, when coexisting SST anomalies outside of the Indian Ocean are removed, MJO precipitation anomalies and propagation speed of 2006IO more closely resemble the behavior in CLIM. When coexisting +IOD SST perturbations are confined to the equatorial Pacific Ocean (2006Pac, Figure 1g), the MJO becomes severely disrupted near 110°E with almost no discernible signal in the Pacific basin.

In summary, Figure 1 interestingly suggests that MJO propagation, at least in the context of the October 2006 +IOD case, is more sensitive to the coexisting SST perturbation in the equatorial Pacific rather than SSTs local to the Indian Ocean.

3.2. Mean State

In this subsection, we analyze the simulated basic state, focusing especially on two key questions: (1) what, if any, important changes in time-mean vertical wind shear or mean moisture occur that might reasonably have implications for MJO propagation; and (2) to what degree is the MJO disruption tropically versus extratropically mediated?

We begin by analyzing the background vertical profile of zonal wind, which can strongly affect tropical intraseasonal disturbance propagation [*Wang and Xie*, 1996; *Inness et al*., 2003; *Sooraj et al*., 2009; *Dias and Kiladis*, 2014]. Figure 2c displays time-mean 850 hPa zonal wind (hereafter, "U850") and Figure 2d vertical shear of the zonal wind, defined as the zonal wind at 200 hPa minus that at 850 hPa (hereafter, "USHEAR") for CLIM. For reference, U850 and USHEAR plots from ECMWF Interim reanalysis (ERA-I) [*Dee et al*., 2011] are shown in Figures 2a and 2b, respectively; however, caution should be taken because the time period selected to compute climatological SST forcing for CLIM (1965–2012) extends well beyond the ERA-I time span used (1979–2014). The simulated continuous zone of equatorial westerlies from 50°to 165°E and concurrent region of easterly USHEAR are qualitatively consistent with climatological October ERA-I winds, but SPCAM underrepresents (overdoes) both U850 and USHEAR magnitudes over the Indian Ocean (West Pacific) by ~2–3 m s^{-1}.

Several realistic aspects of the mean zonal wind response to +IOD conditions build further confidence in SPCAM as a valid tool to study MJO-IOD interactions. U850 time mean (contours) and its difference from CLIM (color shading) are shown for each SPCAM simulation in Figures 2e, 2g, and 2i. SPCAM is able to

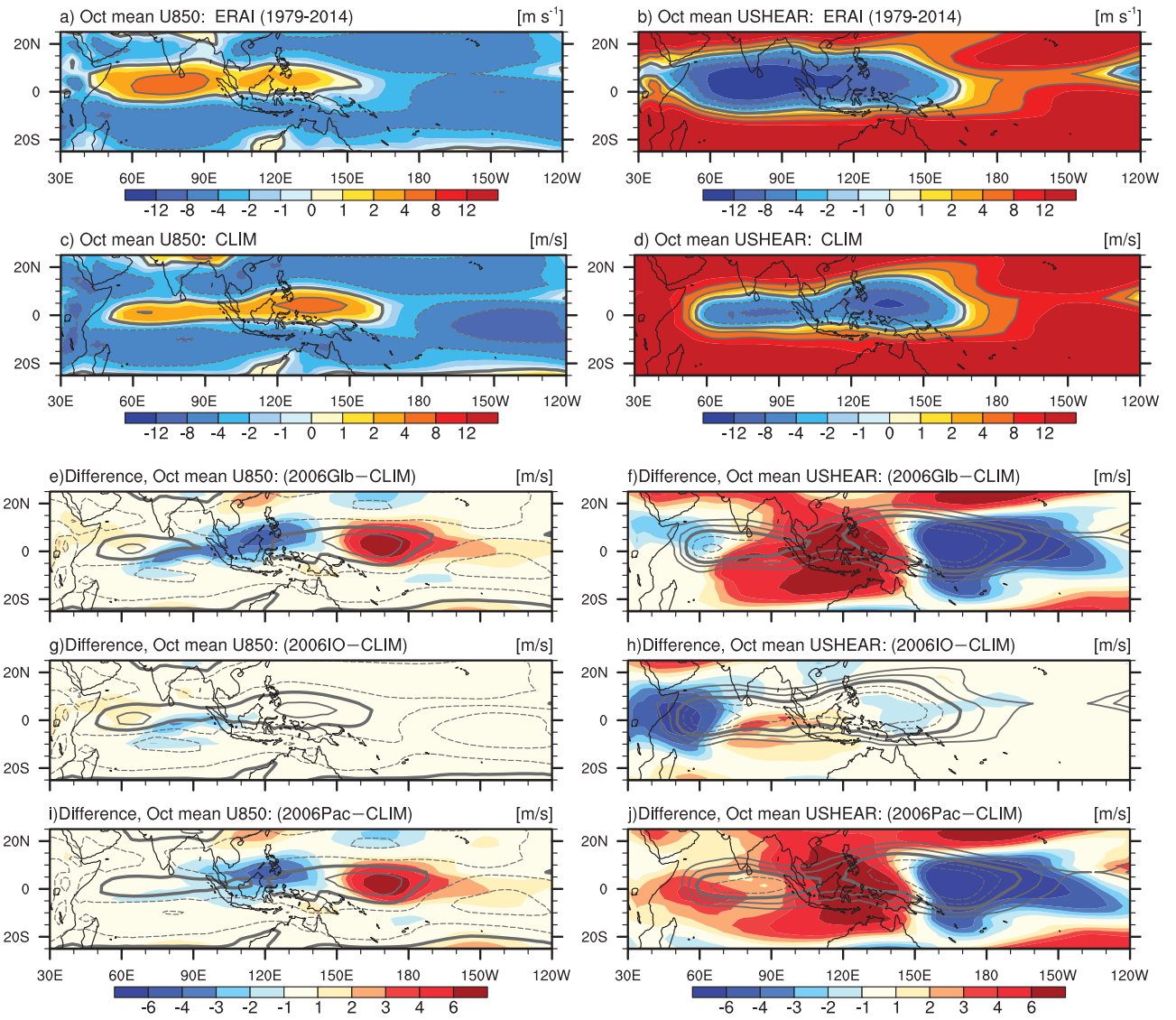

Figure 2. (left column) October mean 850 hPa zonal wind (U850; both shading and contours) for (a) ERA-Interim Reanalysis and (c) CLIM, and (e, g, i) the mean (contours) and its difference from CLIM (color shading) for each experimental simulation. Contour interval is 4 m s^{-1} and negative (zero, positive) contours are dashed (thick solid, thin solid). (right column): As in the left column, but for vertical shear of the zonal wind, defined as U200–U850.

reproduce the +IOD zonal wind profile changes measured from radiosondes at Gan Island (0.7°S, 73.2°E) during the 2006 MISMO field campaign (Figure 3, top row). Local time-mean changes in equatorial U850 follow SST-driven precipitation shifts (cf. Figure 1) in agreement with the expected circulation response to anomalous latent heating [e.g., *Gill*, 1980]. MJO disruption in 2006Glb and 2006Pac (cf. Figures 1d, 1h, 2e, and 2i) is associated with negative U850 anomalies and a reversal from low-level westerlies to easterlies near Indonesia. 2006IO, which has only modest MJO weakening near Indonesia, maintains a continuous zone of equatorial U850 westerlies across the Indo-Pacific.

Comparing Figures 1 and 2, the initial disruption of MJO eastward propagation in 2006Glb and 2006Pac coincides with positive USHEAR anomalies and a reversal from easterly to westerly shear near 110°−120°E (cf. Figures 1d, 1h, 2f, and 2j). With the exception of the far west Indian Ocean, USHEAR anomalies are substantially weaker in 2006IO, which maintains both easterly shear and a robust MJO signal over the Maritime Continent region (cf. Figures 1f and 2h).

It can be tempting to infer from Figure 2 that USHEAR and not U850 has stronger control over MJO propagation, consistent with the fact that the zonal subregion of MJO disruption in 2006Glb (~110°−120°E;

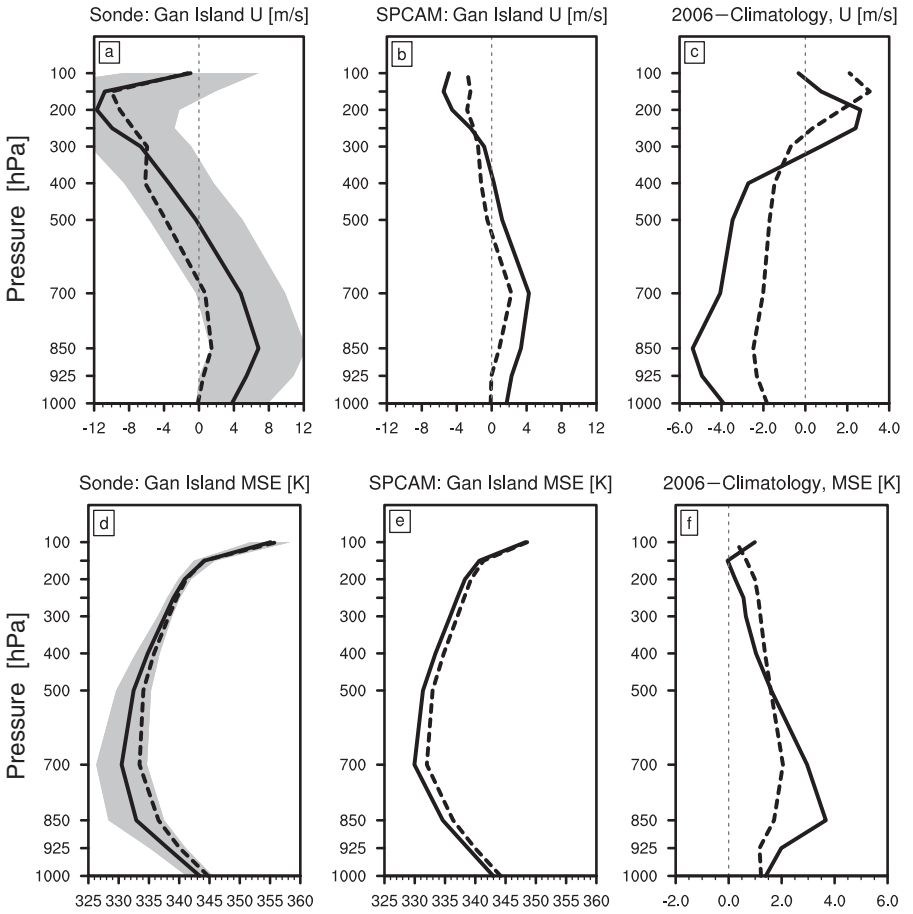

Figure 3. (a) Long-term climatological zonal wind (U) for the boreal fall period from radiosonde data at Gan Island (0.7°S, 73.2°E) (solid black), its $\pm 1\sigma$ range (gray shading), and the 2006 boreal fall mean (dashed black). Boreal fall period is defined here as 22 September to 31 December to span the MISMO field campaign. (b) Time mean U from SPCAM CLIM (solid black) and 2006Glb (dashed black) simulations at (1.4°S, 73.1°E), the model grid point nearest Gan Island. (c) The difference of boreal fall means between 2006 and the long-term climatology for Gan Island radiosonde data (solid black) and the CLIM–2006Glb difference (dashed black). (d–f) As in the top row, but for moist static energy.

Figure 1d) more closely matches that of USHEAR reversal rather than U850 reversal (Figures 2e and 2f, respectively). This is further consistent with *Sooraj et al*. [2009], who noted that subseasonal variability is more strongly dependent on vertical shear structure rather than U850 magnitude. However, we will also argue that other factors such as moisture availability may be especially important.

Additional realistic aspects of the basic state circulation and moisture content can be seen in Figure 4. Longitudinal cross sections of differences in vertical pressure velocity (contours) and moist static energy (MSE; color shading) between 2006Glb and CLIM (Figure 4a) indicate strong subsidence anomalies and reduced MSE over the Maritime Continent bookended by anomalous rising motion and enhanced MSE. The fact that SPCAM reproduces +IOD-driven MSE profile changes reminiscent of that observed from MISMO radiosondes over the Indian Ocean (Figure 3, bottom row) is once again reassuring of its validity as a tool to study IOD-MJO interactions. The region of enhanced subsidence and, in particular, reduced MSE in both 2006Glb and 2006Pac (Figures 4a and 4c) coincides with MJO weakening (Figures 1d and 1h). Interestingly, moderate positive MSE differences extend west of 110°E in 2006Pac despite SST anomalies being restricted to the Pacific Ocean, suggesting that the Pacific SST anomalies are of a magnitude and spatial scale sufficient to affect large-scale circulations in remote Tropical regions. Smaller differences, mainly west of Indonesia, exist in 2006IO (Figure 4b).

Corresponding 850 hPa vector wind and MSE differences between each experimental run and CLIM (Figure 4, right column) reveal that the lower-tropospheric dryness near the Maritime Continent in 2006Glb and 2006Pac (Figures 4d and 4f) is associated with enhanced Rossby gyres centered at (15°N, 130°E) and

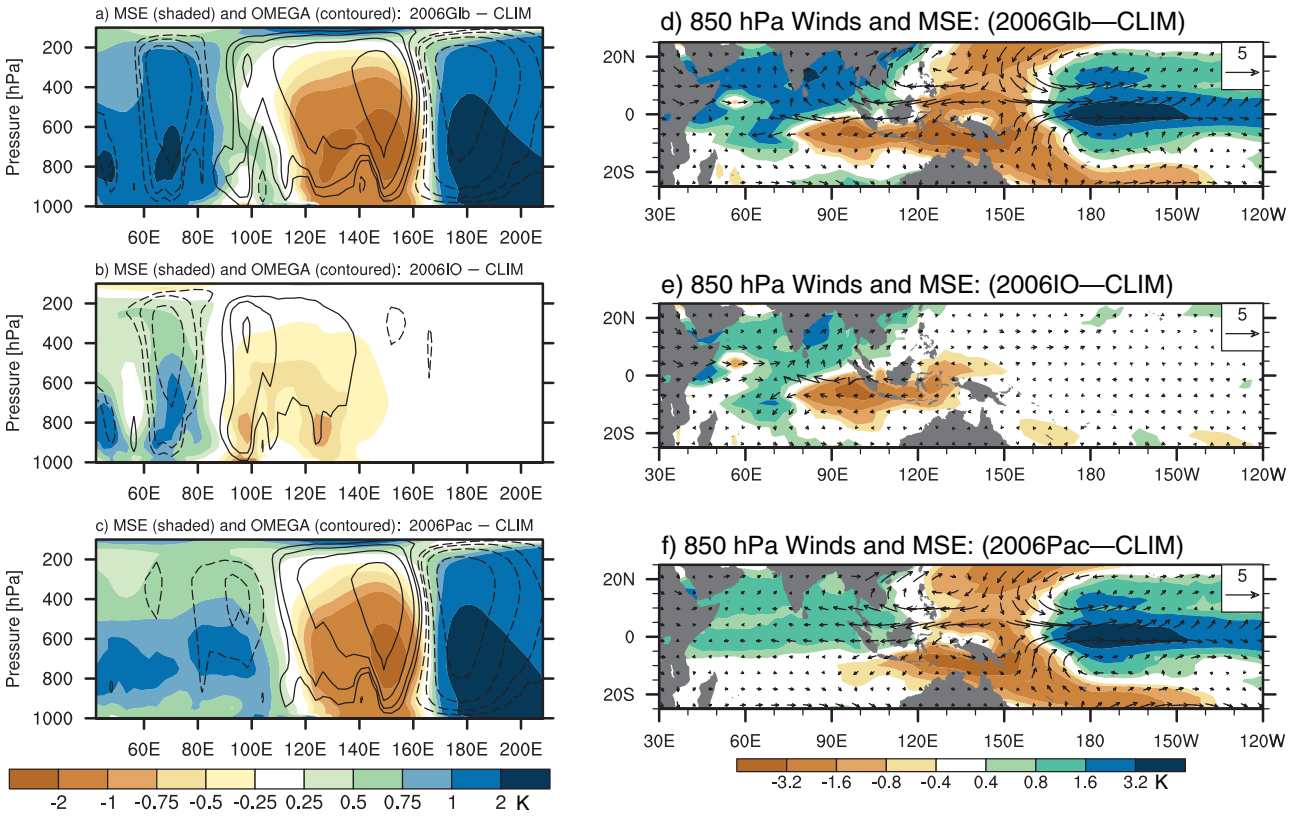

Figure 4. (left column) Longitude-pressure difference from CLIM of mean moist static energy (color shading, converted to temperature units) and vertical pressure velocity (contours) for (a) 2006Glb, (b) 2006IO, and (c) 2006Pac. Data have been averaged from 7°S to 15°N. Pressure velocity contour levels are ±(0.005, 0.01, 0.02, 0.04) Pa s^{-1} and no zero contour is drawn. (right column): Difference from CLIM of mean 850 hPa moist static energy (color shading, in temperature units) and 850 hPa vector winds (arrows, m/s) for (d) 2006Glb, (e) 2006IO, and (f) 2006Pac. Reference wind vector appears in top right corner of each right-column plot.

(15°N, 170°E) with weaker gyres in the Southern Hemisphere. We note that moisture content strongly controls MSE in the tropical lower troposphere. The "moisture mode" hypothesis, one of several theories describing the MJO, posits that MJO convection is strongly dependent on moisture distribution and transport [e.g., *Sobel and Maloney*, 2013]. The enhanced Rossby gyres seen in 2006Glb and 2006Pac import lower-MSE air into the Maritime Continent region that contributes to MJO convective suppression; indeed, this is the case (Figures 1d and 1h). Little MJO disruption is noted in 2006IO, which has no Rossby response in the western Pacific basin and negative MSE anomalies confined to the Maritime Continent mainly south of the Equator (Figure 4e).

In summary, Figures 2 and 4 reveal important clues regarding the two questions posed at the beginning of this mean state analysis. First, time-mean changes of USHEAR (reversal from easterly to westerly vertical shear), vertical motion (enhanced subsidence), and MSE (reduction) are strongly linked to the MJO propagation disruption that occurs near 110°−120°E in 2006Glb and 2006Pac. This potentially implicates both dynamic and thermodynamic basic state responses in mediating the IOD-induced MJO disruption. Second, the time-mean Tropical circulation and thermodynamic difference patterns in 2006Glb result mainly from anomalous SST forcing in the equatorial Indo-Pacific region with only a marginal influence from extratropical SST perturbations. That is, the 2006Glb vertical pressure velocity and MSE anomaly patterns (Figure 4) closely resemble a simple summation of structures from 2006IO and 2006Pac.

3.3. MJO and Subseasonal Variability

We now analyze the simulated MJO to further investigate the mechanisms involved in IOD-induced MJO disruption, beyond the mean state. Our MJO analysis method is inspired by recent literature from moisture mode theory in which mechanisms that modulate column humidity (nearly equivalent to column MSE in the weak temperature gradient environment of the Tropics) [*Sobel et al.*, 2001] are a key component in

controlling MJO behavior [*Yu and Neelin*, 1994; *Sobel et al*., 2001; *Fuchs and Raymond*, 2002, 2005; *Sugiyama*, 2009a,b; *Maloney*, 2009; *Raymond et al*., 2009; *Raymond and Fuchs*, 2009; *Hannah and Maloney*, 2011; *Sobel and Maloney*, 2012, 2013; *Chikira and Sugiyama*, 2013; *Chikira*, 2014; *Sobel et al*., 2014]. From this view, analysis of intraseasonal anomalies in the column MSE budget is an important vantage point for understanding MJO maintenance and propagation mechanisms.

The anomalous column MSE budget is, from *Neelin and Held* [1987]:

$$[\partial m/\partial t] = -[\omega \partial m/\partial p] - [\mathbf{v} \cdot \nabla m] + \mathrm{SH} + \mathrm{LH} + [\mathrm{SW}] + [\mathrm{LW}] \quad (1)$$

where $[\bullet]$ represent mass-weighted integrals between 100 hPa and the surface; m is MSE; ω vertical pressure velocity; $\mathbf{v}$ and ∇ are the horizontal vector wind and gradient operator on a constant pressure surface; SH and LH the surface sensible and latent heat fluxes, respectively; and SW and LW the shortwave and longwave radiation fluxes, respectively. Each term in (1) represents a departure from the seasonal cycle, as noted at the beginning of section 3.1. For simplicity, and to avoid confusion related to forthcoming equations, we have omitted primes from these anomaly terms. Composite SH and [SW] have magnitudes $<|2.5|$ W m^{-2} and are omitted from the budget analysis. Column MSE budget residual magnitudes average 6.2 W m^{-2} between 70° and 90°E and 2.6 W m^{-2} between 120° and 140°E.

We begin by analyzing the left hand side of (1) to verify the MSE compositing methodology. Composites in Figures 5 and 6 are constructed as follows: As described in section 2, each MJO event is fitted with an optimal linear propagation speed line which provides time and longitude trajectory information. For a selected longitude, the time at which each MJO trajectory intersects that longitude is known and can serve as a (0 day lag) base point for a composite. This method accommodates phase speed differences among individual MJO events. Composite anomalies of the dominant column-integrated MSE budget terms occurring when MJO deep convection trajectories intersect 90°E at zero lag day (i.e., when MJO deep convection is centered over the eastern equatorial Indian Ocean) are shown in Figure 5a for each simulation. From the resulting longitudinal composite profile, only selected longitude zones are plotted. Within and immediately west of the MJO convectively active region (Figure 5a, left), $-[\omega \partial m/\partial p]$ and $-[\mathbf{v} \cdot \nabla m]$, the vertical and horizontal MSE transport terms, combine to make $[\partial m/\partial t]$, the MSE time tendency, negative despite counteracting positive column MSE contributions from LH and [LW]. Statistical significance is assessed by comparing, for each budget term, the difference of composited values between individual model pairs to a zero-difference null hypothesis in a Student's *t* test. Plotting the significance metrics among each model pair is intractable; instead, only features exceeding defined significance thresholds will be discussed. Statistically significant intermodel (robust versus disrupted MJO models) differences exceeding the 95% threshold exist for the individual terms driving $[\partial m/\partial t]$ but little model spread is seen in $[\partial m/\partial t]$ itself. Overall, the MSE budget partitioning on Figure 5a (left) is in qualitative agreement with the reanalysis-based results of *Kiranmayi and Maloney* [2011], reassuring us that a satisfactory vantage point from which to analyze the MJO MSE budget has been achieved.

Next, to hone in on propagation dynamics, we examine composite MSE tendencies in the region ahead of MJO deep convection—that is, focusing especially on the longitudes at which MJO disruption occurs in 2006Glb and 2006Pac: ~120°−140°E (Figure 5a, right). This is intended to help highlight mechanisms related to changes in MJO propagation across the simulations, recognizing that accumulation of MSE east of the MJO deep convection center is fundamental to the observed disturbance [e.g., *Kemball-Cook and Weare*, 2001; *Kiladis et al*., 2005; *Kiranmayi and Maloney*, 2011; *Sobel et al*., 2014]. The accumulation is associated with robust MJO eastward propagation in climate model simulations [*Maloney*, 2009; *Benedict and Randall*, 2009; *Cai et al*., 2013a; *Andersen and Kuang*, 2012] and so is expected to varying degrees in all simulations presented here, though possibly affected by IOD-induced disruption. Differences in MJO suppressed-phase $[\partial m/\partial t]$ between CLIM and both models with disrupted MJO signals (2006Glb and 2006Pac) exceed the 95% significance level (Figure 5a, right) and reaffirm that large-scale buildup of MSE ahead of the MJO is associated with robust eastward propagation in all simulations, consistent with moisture mode theory.

We next identify horizontal MSE advection as an important mechanism that disproportionately maintains MJO propagation signals, through composite analysis of the individual column MSE budget terms (right hand side of (1)). Overall, the phasing and amplitude among each of the column MSE budget terms in CLIM

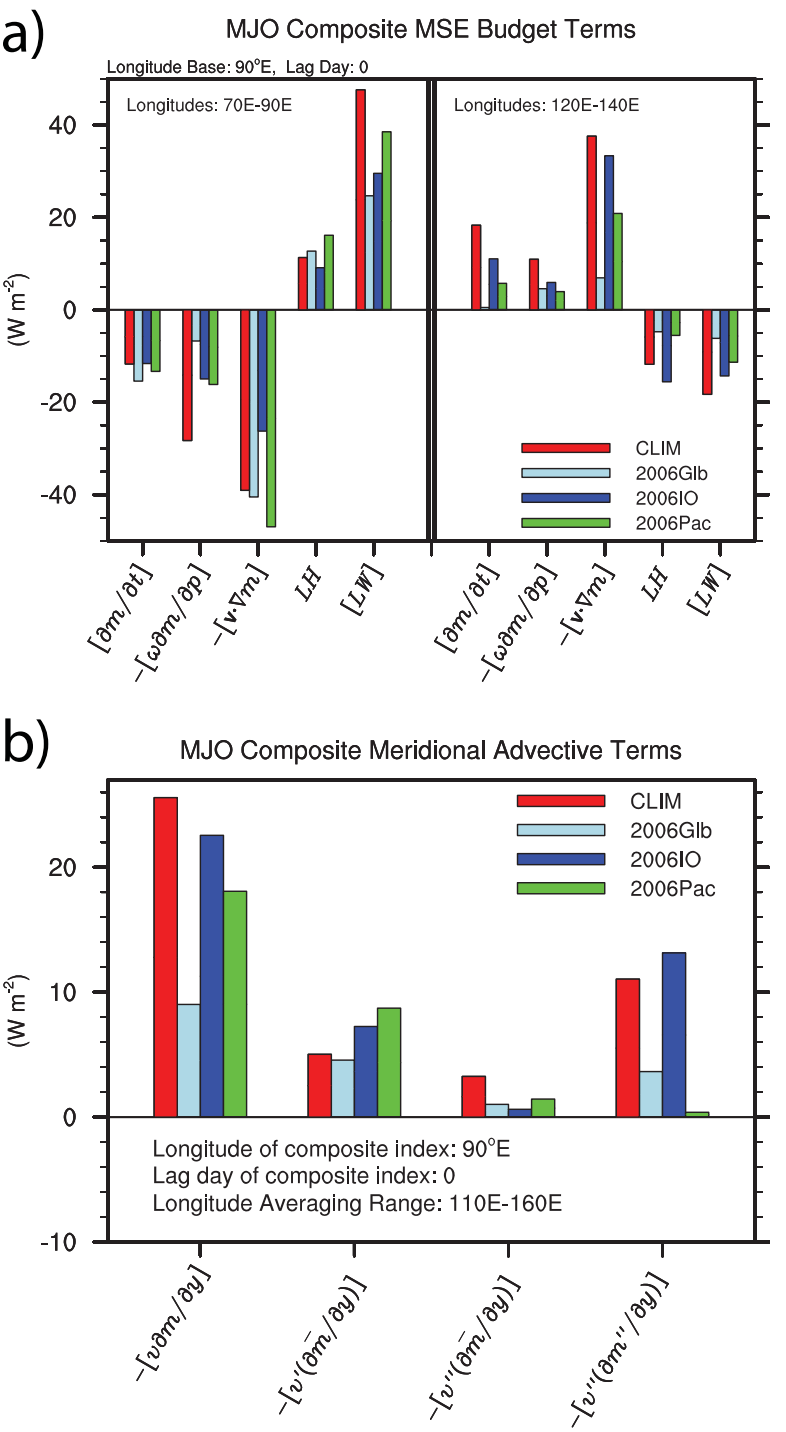

Figure 5. (a) MJO composite anomalies of the dominant terms of the vertically integrated moist static energy (MSE) budget. Data shown represent conditions when MJO deep convection trajectories intersect 90° E at zero lag day (i.e., when MJO deep convection is centered over the eastern equatorial Indian Ocean). Budget terms are averaged from 7° S to 15° N and further averaged between (left) 70° and 90° E within the convectively active phase and (right) 120°-140° E within the convectively suppressed phase. [•] terms are mass-weighted integrals from 100 hPa-surface. (b) As in Figure 5a but for selected timescale-partitioned components of MJO composite meridional MSE advection averaged from 110° to 160° E within the convectively suppressed phase. Overbars represent a 51 day running mean and single (double) primes represent variability on the 17–51 day (2–17 day) time scale. See text for term descriptions.

and 2006IO, the simulations with limited MJO weakening, are more pronounced compared to 2006Glb and 2006Pac (Figure 5a, right). Key intersimulation differences arise in composite $-[\mathbf{v} \cdot \nabla m]$, the dominant contributor to column MSE increase at this stage of the MJO life cycle, and thus highlight the importance of

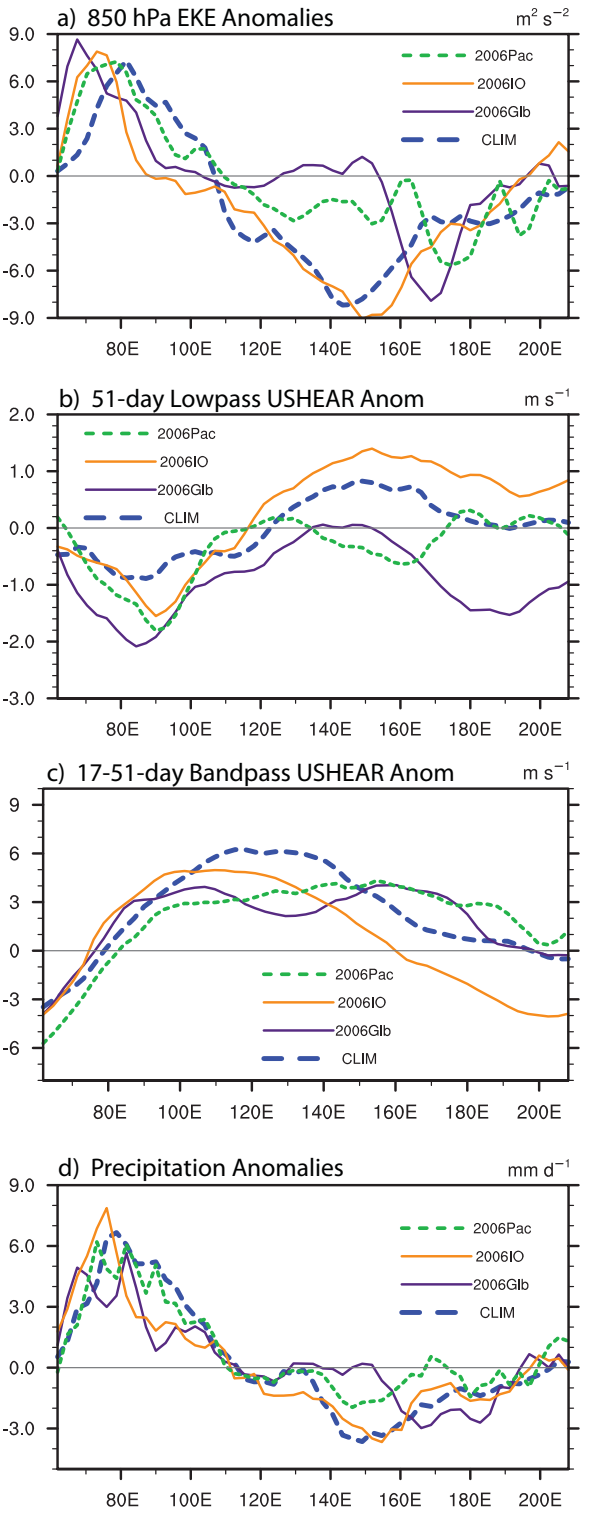

Figure 6. Composite anomalies of (a) 850 hPa eddy kinetic energy, (b), MJO background (51 day low-pass filtered) vertical shear of the zonal wind (USHEAR), (c) eddy background (17–51 day band-pass filtered) USHEAR, and (d) precipitation. Plotted longitudinal profiles represent an average over lag days +5 to +10 relative to the date at which MJO deep convection initiates in the western Indian Ocean, as shown in Figure 1. See text for details and variable descriptions.

horizontal moisture advection to MJO maintenance and propagation. CLIM-2006Glb and 2006IO-2006Glb differences are statistically robust (exceed 99% threshold) but CLIM-2006Pac and 2006IO-2006Pac differences are only marginally significant (exceed 90% threshold) partly owing to the smaller sample size of 2006Pac.

Ultimately, a detailed decomposition reveals meridional advection of MSE by submonthly MJO eddies as a primary mechanism involved in IOD-induced MJO disruption. Following *Maloney* [2009], anomalous horizontal MSE advection associated with MJO dynamics can be decomposed into zonal $-u(\partial m/\partial x)$ and meridional $-v(\partial m/\partial y)$ components, with the meridional term being dominant for the MJO composites examined here (not shown) [see, e.g., *Andersen and Kuang*, 2012]. Further partitioning of the anomalous meridional advection term into various time scales results in:

$$-v\frac{\partial m}{\partial y} = -(\bar{v}+v'+v'')\frac{\partial}{\partial y}(\bar{m}+m'+m'') \quad (2)$$

where overbars denote a 51 day running average ("background variability"), x' denotes variability of x on the 17–51 day time scale computed using a band-pass filter ("MJO variability"), and x'' denotes variability of x on time scales less than 17 days computed using a high-pass filter ("eddy variability"). Double-primed terms represent submonthly synoptic and mesoscale eddies. The terms in (2) have magnitude maxima near and below the mid-troposphere where the largest horizontal moisture gradients exist (not shown) and are generally positively correlated with height, suggesting that a vertical integral can represents well the spatial distribution of meridional MSE advection. Each term in (2) is integrated from 100 hPa to the surface, anomalies are computed, MJO composites are constructed as in Figure 5a, and the resulting longitudinal composite snapshot is averaged from 110°to 160°E within the broad convectively suppressed phase. Composite residual magnitudes of (2) have an average $<|0.5|$ W m^{-2} and a maximum $<|2.5|$ W m^{-2}. Most of the nine terms from the rhs expansion of the vertically integrated form of (2) contribute little to $-[v(\partial m/\partial y)]$ (where $[\bullet]$ represents the mass-weighted integral). The largest contributors that shape the behavior of $-[v(\partial m/\partial y)]$ are $-[v''(\partial m''/\partial y)]$ (synoptic and mesoscale

eddies), $-[v''(\partial\bar{m}/\partial y)]$ (eddy winds acting on the background meridional MSE gradient), and $-[v'(\partial\bar{m}/\partial y)]$ (MJO-scale winds acting on the background meridional MSE gradient). These dominant components are shown in Figure 5b and indicate very different behavior among the simulations. CLIM and 2006IO show a similar pattern of enhanced MSE due to strong anomalous meridional advection ($-[v(\partial m/\partial y)]$) that is primarily on eddy scales ($-[v''(\partial m''/\partial y)]$) and, to a lesser extent, related to MJO-scale winds acting on the background meridional MSE gradient ($-[v'(\partial\bar{m}/\partial y)]$). The magnitude of $-[v(\partial m/\partial y)]$ in 2006Pac has a similar magnitude to that of CLIM and 2006IO, but this MSE increase is dominated by MJO-scale winds acting on the background MSE gradient with nearly zero anomalous contribution on eddy scales ($-[v''(\partial m''/\partial y)]$). 2006Glb has weak meridional MSE advection overall, particularly related to eddy activity. The disparity in $-[v''(\partial m''/\partial y)]$ between model pairs exceeds the 95% significance threshold.

Given the apparent importance of synoptic and mesoscale eddies in controlling MJO column MSE anomalies, composite longitudinal snapshots of anomalous 850 hPa eddy kinetic energy (EKE) at the time when MJO deep convection is propagating across the equatorial central Indian Ocean are shown in Figure 6a. The plotted composite longitudinal profiles represent an average over lag days +5 to +10 relative to Day 0 as defined in section 2 when MJO deep convection initiates over the western Indian Ocean (i.e., when West Pacific MJO deep convection is strongly suppressed, see Figure 1). EKE is defined as $(\tilde{u}^2+\tilde{v}^2)/2$, where $\tilde{x}$ is the departure from an 11 day running mean of x. All simulations have enhanced EKE near and west of MJO deep convection (40°−90°E), as referenced from corresponding precipitation anomalies shown in Figure 6d. The key distinguishing feature of Figure 6a is the lack of EKE suppression over the Maritime Continent and West Pacific regions in 2006Glb and 2006Pac, which have severe MJO disruption. This MJO disruption first emerges near 110°−120°E, matching the longitude at which composite anomalous EKE begins to diverge among the simulations (cf. Figures 1 and 6a). Sustained eddy activity during the MJO suppressed phase in 2006Glb and 2006Pac is linked to weaker meridional eddy moistening (stronger eddy drying; Figure 5b) and ultimately contributes to weaker column MSE accumulation (Figure 5a) compared to simulations with robust MJO propagation (CLIM and 2006IO). The overactive eddies exist within a stronger easterly USHEAR environment. Figures 6b and 6c show USHEAR composite anomalies on the "MJO-background" time scale, computed using a 51 day low-pass filter, and the "eddy-background" time scale, computed using a 17–51 day band-pass filter, respectively. On both background time scales, anomalous easterly shear is evident for the MJO-disrupted simulations (2006Glb and 2006Pac) straddling the longitude range of stronger low-level EKE, supporting previous studies [e.g., *Sooraj et al*., 2009]. Further discussion on eddy interactions with the intraseasonal zonal wind profile will be presented in section 4.

4. Summary and Discussion

A suite of four superparameterized CAM (version 3.0; SPCAM) simulations forced with idealized variants of the October 2006 positive Indian Ocean Dipole (+IOD) SST anomaly pattern reveal significant MJO propagation differences. SPCAM is demonstrated as a useful tool for studying mechanisms involved in IOD-induced MJO disruption in that its intrinsic perpetual-October MJO (case "CLIM"; Figure 1b) is realistically disrupted near the Maritime Continent when the model is forced instead with +IOD October 2006 SST anomalies. This disruption occurs if SSTs are modified by the +IOD anomaly either globally (case "2006Glb") or restricted to the equatorial Pacific Ocean (case "2006Pac")—in each case, severe weakening of the MJO precipitation signal occurs over the Maritime Continent between 110° and 140°E and the disturbance speed increases across the West Pacific (Figures 1d and 1h) [*Wilson et al*., 2013]. But when +IOD October 2006 SST anomalies are applied only in the equatorial Indian Ocean (case "2006IO"), robust MJO eastward propagation is "recovered" and only limited weakening of the signal occurs over the Maritime Continent (Figure 1f).

MJO disruption in 2006Glb and 2006Pac is associated with changes in the background wind and thermodynamic fields as well as reduced effectiveness of horizontal advective moist static energy (MSE) accumulation ahead of MJO deep convection on subseasonal scales. The longitudes where MJO disruption occurs in 2006Glb and 2006Pac (∼110°−120°E) match the location where time-mean equatorial 850 hPa zonal winds (U850) reverse from westerlies to easterlies (Figure 2, left); easterly vertical shear of the zonal wind (USHEAR) weakens or reverses (Figure 2, right); and subsiding, lower-MSE air is imported from the subtropics driven by Rossby-like gyres (Figure 4). On subseasonal scales, significantly limited accumulations of MSE—primarily resulting from weaker meridional advective moistening—occur ahead of MJO deep convection and impede

its eastward propagation. The weaker meridional moistening is attributed to persistent submonthly eddy activity within an anomalously easterly sheared environment. The enhanced eddy activity permits mixing of drier subtropical air into the path of MJO deep convection and thus produces unfavorable conditions for sustained MJO eastward propagation.

Numerous caveats of this study must be acknowledged:

1. Atmospheric forcing from MJO disturbances significantly impacts the upper ocean on intraseasonal and interannual time scales and can generate subsequent feedbacks onto the atmosphere [*Waliser et al*., 2003; *Han et al*., 2004; *Duncan and Han*, 2012; see *Kessler*, 2005; *DeMott et al*., 2015 reviews]. The absence of realistic air-sea interaction is a clear limitation of the present study. This could be viewed as a disadvantage, since interactive SSTs generally improve the MJO signal in climate models [*Waliser et al*., 1999; *Stan et al*., 2010; *Benedict and Randall*, 2011] and enable full land-atmosphere-sea surface interactions to unfold. But our use of temporally constant SSTs has complementary practical advantages in that it optimizes MJO detectability in a computationally intensive superparameterized climate model. Additionally, eliminating seasonality clarifies the atmospheric response to idealized oceanic forcing, helping increase MJO sample size relative to seasonally varying SST forcing.
2. The quantitative assessment of the DMI could be improved [e.g., *Werner et al*., 2012]. Subsurface (rather than surface) ocean temperatures were found to better discriminate internally generated IOD fluctuations from ENSO-driven impacts [*Shinoda et al*., 2004; *Zhao and Nigam*, 2015]. It would be worth exploring whether our finding of an insensitivity of MJO propagation to +IOD SSTs localized to the Indian Ocean is robust to the choice of IOD index.
3. Our analysis focuses on a single +IOD SST realization: October 2006 monthly mean. On the one hand, this +IOD event is highly amplified (as measured by SST) [*Horii et al*., 2008; *Wilson et al*., 2013] to optimize detectability and was chosen since it is representative of canonical +IOD conditions [*Saji and Yamagata*, 2003]; on the other hand, it would be worth investigating the robustness of the IOD responses documented in this paper to an ensemble of IOD events. Although beyond the scope of this study, this would be possible in less computationally demanding, conventionally parameterized but MJO-permitting GCMs. To reproduce the observed MJO response to +IOD SST forcing, such models would likely need to have a fair representation of the MJO and the ability to accurately simulate the mean state moisture, circulation, and stability responses to the SST perturbation. It is possible that models might also require a realistic representation of submonthly processes and their response to the IOD. Achieving an accurate depiction of mean state, intraseasonal, and submonthly disturbances and the interaction between them poses a major challenge to many conventionally parameterized GCMs [*Jiang et al*., 2015].
4. An unknown sensitivity to the SST weighting mask geometry exists, but computational resources currently limit a more rigorous sensitivity analysis. The mask was constructed to capture emergent basin-scale SST features in the Indian and Pacific Oceans within a meridional range spanning latitudes of greatest MJO activity.
5. The MJO composite sample sizes—particularly for 2006Pac (11 events)—are marginally acceptable. This disadvantage has been hedged against by using a modern MJO identification scheme that nonetheless successfully isolates the most intense events producing clear propagation composites even in a limited sample, but we acknowledge even longer simulations would have been preferable.

Despite these limitations, several new and important contributions toward an improved understanding of how interannual SSTs influence the MJO are evident. The SPCAM forced with prescribed +IOD SSTs is able to reproduce observed atmospheric changes in the seasonal mean [*Saji et al*., 1999] and the MJO [*Wilson et al*., 2013]. More severe MJO weakening noted in Figure 1d compared to Figure 7 of *Wilson et al*. [2013] likely arises because that study combines numerous +IOD cases of varying intensity whereas ours covers a single, amplified, but representative realization of +IOD conditions.

This study demonstrates that IOD-driven impacts on MJO propagation emerge over a range of time scales. SSTs associated with +IOD conditions reduce background (in this case, seasonal to interannual) lower-tropospheric MSE (akin to moisture) by driving circulations that subside over the Maritime Continent and import drier subtropical air. Reduced background lower-tropospheric moisture near Indonesia associated with +IOD SSTs has been linked to weakened MJO propagation [*Wilson et al*., 2013] and suppressed subseasonal convection and zonal wind variability [*Shinoda and Han*, 2005]. However, the critical role of background low-level zonal wind and, perhaps more importantly, the vertical shear of the zonal wind for MJO

propagation are also evident in our results. These findings are consistent with *Kug et al*. [2009] and *Sooraj et al*. [2009] who show that a transition to more westerly vertical shear of the background zonal wind during +IOD reduces observed and simulated MJO variability, respectively.

Our analysis indicates that multiscale subseasonal processes are also impacted by +IOD SSTs. During such conditions, a lack of column MSE accumulation ahead of MJO deep convection is associated with weaker horizontal MSE convergence driven in part by anomalously active submonthly meridional eddy mixing that entrains drier subtropical air into the Tropics. The fact that MSE transport and accumulation play a vital role in MJO propagation lends support to moisture mode theory [*Sobel et al*., 2001]. The overactive eddy mixing occurs with anomalous easterly vertical shear of the zonal wind during the MJO suppressed phase. *Shinoda and Han* [2005] find that submonthly variability is reduced rather than enhanced over the eastern equatorial Indian Ocean during +IOD conditions. However, those authors did not composite their results based on MJO phase as we have done. *Kug et al*. [2009] and *Sooraj et al*. [2009] also note that submonthly wind variability is negatively correlated with the IOD, but moisture fields were not examined in those studies as they are here.

The prominent role of synoptic eddy activity in modulating MJO energetics and moisture has been reported previously [*Maloney and Dickinson*, 2003; *Maloney*, 2009; *Kiranmayi and Maloney*, 2011; *Andersen and Kuang*, 2012; *Sobel and Maloney*, 2013]. Our results generally support these studies and, in addition, highlight the impact of SST-driven mean state changes on both intraseasonal and submonthly disturbances, underscoring the contribution of multiscale interactions in determining MJO moisture availability, maintenance, and propagation. Our findings suggest that eddy mixing ahead of MJO deep convection, if not sufficiently suppressed, can strongly contribute to MJO weakening and disruption.

Finally, our results demonstrate that boreal fall +IOD SST perturbations local to the Indian Ocean have a significantly smaller impact on MJO deep convection propagation across the Maritime Continent compared to contemporaneous SST anomalies within the equatorial Pacific Ocean, which for the October 2006 case resemble El Niño-like conditions [cf. *Harrison and Larkin*, 1998, Figure 1c and Plate 3]. *Shinoda and Han* [2005] speculate that the weaker correlation between 30 and 90 day variability of Indian Ocean deep convection (compared to 6–30 day variability) and the DMI might arise because (1) the spatial scale of IOD SST perturbations is not sufficiently broad to impact the planetary-scale MJO or (2) the IOD SST anomalies might not exist long enough to strongly influence the MJO. Our results, derived from using 15 years of fixed-SST +IOD conditions, clearly support the former hypothesis but suggest that the time scale of amplified Indian Ocean +IOD SST anomalies—even if applied continuously for 15 years—is not a major factor for MJO propagation.

The limited influence of +IOD SSTs within the Indian Ocean on MJO propagation across the Maritime Continent may result from the geographic location of minimum SST anomalies or the misaligned maxima in seasonal DMI extremes and MJO activity. For both the October 2006 +IOD case (Figure 1) and in a +IOD SST composite [see *Saji and Yamagata*, 2003], the coolest +IOD SST anomalies reside along Sumatra's west coast mostly south of the Equator. However, a band of neutral or slightly positive anomalies exists just north of this SST minimum (Figure 1e) and appears sufficient to sustain MJO activity along this north-shifted corridor as noted in plots of 20–100 day band-pass filtered precipitation and 850 hPa zonal wind variance (not shown). The seasonal MJO peak (boreal winter and spring) [*Zhang and Dong*, 2004] lags the seasonal IOD peak (boreal fall) [*Saji and Yamagata*, 2003], which might also weaken the MJO-IOD connection.

MJO impacts from Pacific SST perturbations—whether related to IOD or ENSO—are clearly evident in this study. MJO-ENSO interactions are well documented [e.g., *Fink and Speth*, 1997], but our understanding of the degree of independence between the IOD and ENSO is still crystallizing [*Zhao and Nigam*, 2015]. Regardless of this relationship, accurate representation of the interaction between the MJO and interannual Pacific SST fluctuations is a vital step toward successfully modeling both Indo-Pacific and global precipitation variability in the present-day and future climate.

Acknowledgments

We thank Hongyan Zhu and one anonymous reviewer for their constructive comments on this manuscript. GPCP precipitation data provided by the NOAA/OAR/ESRL PSD, Boulder, Colorado, USA (http://www.esrl.noaa.gov/psd/). Data discussed in this paper can be made available from the authors upon request. This study used the Extreme Science and Engineering Discovery Environment, which is supported by National Science Foundation (NSF) grant OCI-1053575, under allocation TG-ATM120034. J.B. and W.C. were funded by the U.S. Department of Energy (DOE) Scientific Discovery for Advanced Computing "Multiscale Methods for Accurate, Efficient, and Scale-Aware Models of the Earth System" project. M.P. was funded by NSF grant AGS-1419518 and DOE grants DE-SC0012152 and DE-SC0012548. This study benefitted greatly from discussions with Chidong Zhang, Toshi Shinoda, David Randall, and Charlotte DeMott.

References

Adler, R. F., et al. (2003), The version-2 global precipitation climatology project (gpcp) monthly precipitation analysis (1979-present), *J. Hydrometeorol.*, *4*(6), 1147–1167.

Andersen, J. A., and Z. Kuang (2012), Moist static energy budget of mjo-like disturbances in the atmosphere of a zonally symmetric aquaplanet, *J. Clim.*, *25*(8), 2782–2804.

Arnold, N. P., Z. Kuang, and E. Tziperman (2013), Enhanced mjo-like variability at high sst, *J. Clim.*, *26*(3), 988–1001.
Arnold, N. P., M. Branson, Z. Kuang, D. A. Randall, and E. Tziperman (2015), Mjo intensification with warming in the superparameterized cesm, *J. Clim.*, *28*(7), 2706–2724.
Benedict, J. J., and D. A. Randall (2009), Structure of the Madden-Julian oscillation in the superparameterized cam, *J. Atmos. Sci.*, *66*(11), 3277–3296.
Benedict, J. J., and D. A. Randall (2011), Impacts of idealized air-sea coupling on Madden-Julian oscillation structure in the superparameterized cam, *J. Atmos. Sci.*, *68*(9), 1990–2008.
Bony, S., and K. A. Emanuel (2005), On the role of moist processes in tropical intraseasonal variability: Cloud-radiation and moisture-convection feedbacks, *J. Atmos. Sci.*, *62*(8), 2770–2789.
Cai, Q., G. J. Zhang, and T. Zhou (2013a), Impacts of shallow convection on mjo simulation: A moist static energy and moisture budget analysis, *J. Clim.*, *26*(8), 2417–2431.
Cai, W., X.-T. Zheng, E. Weller, M. Collins, T. Cowan, M. Lengaigne, W. Yu, and T. Yamagata (2013b), Projected response of the Indian ocean dipole to greenhouse warming, *Nat. Geosci.*, *6*(12), 999–1007.
Cai, W., A. Santoso, G. Wang, E. Weller, L. Wu, K. Ashok, Y. Masumoto, and T. Yamagata (2014), Increased frequency of extreme Indian ocean dipole events due to greenhouse warming, *Nature*, *510*(7504), 254–258.
Chikira, M. (2014), Eastward-propagating intraseasonal oscillation represented by Chikira–Sugiyama cumulus parameterization. Part ii: Understanding moisture variation under weak temperature gradient balance, *J. Atmos. Sci.*, *71*(2), 615–639.
Chikira, M., and M. Sugiyama (2013), Eastward-propagating intraseasonal oscillation represented by Chikira–Sugiyama cumulus parameterization. Part i: Comparison with observation and reanalysis, *J. Atmos. Sci.*, *70*(12), 3920–3939.
Dee, D., et al. (2011), The era-interim reanalysis: Configuration and performance of the data assimilation system, *Q. J. R. Meteorol. Soc.*, *137*(656), 553–597.
DeMott, C. A., N. P. Klingaman, and S. J. Woolnough (2015), Atmosphere–ocean coupled processes in the Madden–Julian oscillation, *Rev. Geophys.*, *53*, doi:10.1002/2014RG000478, in press.
Dias, J., and G. N. Kiladis (2014), Influence of the basic state zonal flow on convectively coupled equatorial waves, *Geophys. Res. Lett.*, *41*, 6904–6913, doi:10.1002/2014GL061476.
Dommenget, D. (2011), An objective analysis of the observed spatial structure of the tropical Indian ocean sst variability, *Clim. Dyn.*, *36*(11–12), 2129–2145.
Duncan, B., and W. Han (2012), Influence of atmospheric intraseasonal oscillations on seasonal and interannual variability in the upper Indian ocean, *J. Geophys. Res.*, *117*, C11028, doi:10.1029/2012JC008190.
Fink, A., and P. Speth (1997), Some potential forcing mechanisms of the year-to-year variability of the tropical convection and its intraseasonal (25–70-day) variability, *Int. J. Climatol.*, *17*(14), 1513–1534.
Fischer, A. S., P. Terray, E. Guilyardi, S. Gualdi, and P. Delecluse (2005), Two independent triggers for the Indian ocean dipole/zonal mode in a coupled GCM, *J. Clim.*, *18*(17), 3428–3449.
Fuchs, Ž., and D. J. Raymond (2002), Large-scale modes of a nonrotating atmosphere with water vapor and cloud-radiation feedbacks, *J. Atmos. Sci.*, *59*(10), 1669–1679.
Fuchs, Z., and D. J. Raymond (2005), Large-scale modes in a rotating atmosphere with radiative-convective instability and WISHE, *J. Atmos. Sci.*, *62*(11), 4084–4094.
Gill, A. (1980), Some simple solutions for heat-induced tropical circulation, *Q. J. R. Meteorol. Soc.*, *106*, 447–462.
Grabowski, W. W., and P. K. Smolarkiewicz (1999), CRCP: A cloud resolving convection parameterization for modeling the tropical convecting atmosphere, *Physica D*, *133*(1), 171–178.
Han, W., P. Webster, R. Lukas, P. Hacker, and A. Hu (2004), Impact of atmospheric intraseasonal variability in the Indian ocean: Low-frequency rectification in equatorial surface current and transport, *J. Phys. Oceanogr.*, *34*(6), 1350–1372.
Hannah, W. M., and E. D. Maloney (2011), The role of moisture-convection feedbacks in simulating the Madden-Julian oscillation, *J. Clim.*, *24*(11), 2754–2770.
Harrison, D., and N. K. Larkin (1998), El niño-southern oscillation sea surface temperature and wind anomalies, 1946–1993, *Rev. Geophys.*, *36*(3), 353–399.
Horii, T., H. Hase, I. Ueki, and Y. Masumoto (2008), Oceanic precondition and evolution of the 2006 Indian ocean dipole, *Geophys. Res. Lett.*, *35*, L03607, doi:10.1029/2007GL032464.
Hurrell, J. W., J. J. Hack, D. Shea, J. M. Caron, and J. Rosinski (2008), A new sea surface temperature and sea ice boundary dataset for the community atmosphere model, *J. Clim.*, *21*(19), 5145–5153.
Inness, P. M., J. M. Slingo, E. Guilyardi, and J. Cole (2003), Simulation of the Madden-Julian oscillation in a coupled general circulation model. Part ii: The role of the basic state, *J. Clim.*, *16*(3), 365–382.
Jiang, X., et al. (2015), Vertical structure and physical processes of the Madden-Julian oscillation: Exploring key model physics in climate simulations, *J. Geophys. Res. Atmos.*, *120*, 4718–4748, doi:10.1002/2014JD022375.
Jones, C., and L. Carvalho (2011), Will global warming modify the activity of the Madden–Julian oscillation?, *Q. J. R. Meteorol. Soc.*, *137*(655), 544–552.
Kemball-Cook, S. R., and B. C. Weare (2001), The onset of convection in the Madden-Julian oscillation, *J. Clim.*, *14*(5), 780–793.
Kessler, W. S. (2005), The oceans, in *Intraseasonal Variability in the Atmosphere-Ocean Climate System*, edited by W. K. M. Lau and D. E. Waliser, pp. 175–222, Praxis Publishing Ltd., Chichester, U. K.
Kessler, W. S., and R. Kleeman (2000), Rectification of the Madden-Julian oscillation into the enso cycle, *J. Clim.*, *13*(20), 3560–3575.
Khairoutdinov, M., C. DeMott, and D. Randall (2008), Evaluation of the simulated interannual and subseasonal variability in an AMIP-style simulation using the CSU multiscale modeling framework, *J. Clim.*, *21*(3), 413–431.
Khairoutdinov, M. F., and D. A. Randall (2001), A cloud resolving model as a cloud parameterization in the NCAR community climate system model: Preliminary results, *Geophys. Res. Lett*, *28*(18), 3617–3620.
Khairoutdinov, M. F., and D. A. Randall (2003), Cloud resolving modeling of the arm summer 1997 IOP: Model formulation, results, uncertainties, and sensitivities, *J. Atmos. Sci.*, *60*(4), 607–625.
Kiladis, G. N., K. H. Straub, and P. T. Haertel (2005), Zonal and vertical structure of the Madden-Julian oscillation, *J. Atmos. Sci.*, *62*(8), 2790–2809.
Kiranmayi, L., and E. D. Maloney (2011), Intraseasonal moist static energy budget in reanalysis data, *J. Geophys. Res.*, *116*, D21117, doi:10.1029/2011JD016031.
Klein, S. A., B. J. Soden, and N.-C. Lau (1999), Remote sea surface temperature variations during enso: Evidence for a tropical atmospheric bridge, *J. Clim.*, *12*(4), 917–932.

Kug, J.-S., K. Sooraj, F.-F. Jin, J.-J. Luo, and M. Kwon (2009), Impact of Indian Ocean dipole on high-frequency atmospheric variability over the Indian Ocean, *Atmos. Res.*, *94*(1), 134–139.
Ling, J., C. Zhang, and P. Bechtold (2013), Large-scale distinctions between mjo and non-mjo convective initiation over the tropical indian ocean, *J. Atmos. Sci.*, *70*(9), 2696–2712.
Ling, J., P. Bauer, P. Bechtold, A. Beljaars, R. Forbes, F. Vitart, M. Ulate, and C. Zhang (2014), Global versus local mjo forecast skill of the ECMWF model during DYNAMO, *Mon. Weather Rev.*, *142*(6), 2228–2247.
Maloney, E. D. (2009), The moist static energy budget of a composite tropical intraseasonal oscillation in a climate model, *J. Clim.*, *22*(3), 711–729.
Maloney, E. D., and M. J. Dickinson (2003), The intraseasonal oscillation and the energetics of summertime tropical western north pacific synoptic-scale disturbances, *J. Atmos. Sci.*, *60*(17), 2153–2168.
Maloney, E. D., and S.-P. Xie (2013), Sensitivity of tropical intraseasonal variability to the pattern of climate warming, *J. Adv. Model. Earth Syst.*, *5*, 32–47, doi:10.1029/2012MS000171.
Meyers, G., P. McIntosh, L. Pigot, and M. Pook (2007), The years of el niño, la niña, and interactions with the tropical indian ocean, *J. Clim.*, *20*(13), 2872–2880.
Neelin, J. D., and I. M. Held (1987), Modeling tropical convergence based on the moist static energy budget, *Mon. Weather Rev.*, *115*(1), 3–12.
Okumura, Y. M., and C. Deser (2010), Asymmetry in the duration of el niño and la niña, *J. Clim.*, *23*(21), 5826–5843.
Pritchard, M. S., and C. S. Bretherton (2014), Causal evidence that rotational moisture advection is critical to the superparameterized Madden–Julian oscillation, *J. Atmos. Sci.*, *71*(2), 800–815.
Pritchard, M. S., C. S. Bretherton, and C. A. DeMott (2014), Restricting 32–128 km horizontal scales hardly affects the mjo in the superparameterized community atmosphere model v. 3.0 but the number of cloud-resolving grid columns constrains vertical mixing, *J. Adv. Model. Earth Syst.*, *6*, 723–739, doi:10.1002/2014MS000340.
Raymond, D. J., and Ž. Fuchs (2009), Moisture modes and the Madden-Julian oscillation, *J. Clim.*, *22*(11), 3031–3046.
Raymond, D. J., S. L. Sessions, A. H. Sobel, and Ž. Fuchs (2009), The mechanics of gross moist stability, *J. Adv. Model. Earth Syst.*, *1*, 9, doi: 10.3894/JAMES.2009.1.9.
Reverdin, G., D. L. Cadet, and D. Gutzler (1986), Interannual displacements of convection and surface circulation over the equatorial indian ocean, *Q. J. R. Meteorol. Soc.*, *112*(471), 43–67.
Saji, N., and T. Yamagata (2003), Possible impacts of indian ocean dipole mode events on global climate, *Clim. Res.*, *25*(2), 151–169.
Saji, N. H., B. N. Goswami, P. N. Vinayachandran, and T. Yamagata (1999), A dipole mode in the tropical indian ocean, *Nature*, *401*(6751), 360–363.
Salby, M. L., and H. H. Hendon (1994), Intraseasonal behavior of clouds, temperature, and motion in the tropics, *J. Atmos. Sci.*, *51*(15), 2207–2224.
Schott, F. A., S.-P. Xie, and J. P. McCreary (2009), Indian ocean circulation and climate variability, *Rev. Geophys.*, *47*, RG1002, doi:10.1029/2007RG000245.
Shinoda, T., and W. Han (2005), Influence of the Indian Ocean dipole on atmospheric subseasonal variability, *J. Clim.*, *18*(18), 3891–3909.
Shinoda, T., H. H. Hendon, and M. A. Alexander (2004), Surface and subsurface dipole variability in the Indian ocean and its relation with enso, *Deep Sea Res., Part I*, *51*(5), 619–635.
Sobel, A., and E. Maloney (2012), An idealized semi-empirical framework for modeling the Madden-Julian oscillation, *J. Atmos. Sci.*, *69*(5), 1691–1705.
Sobel, A., and E. Maloney (2013), Moisture modes and the eastward propagation of the mjo, *J. Atmos. Sci.*, *70*(1), 187–192.
Sobel, A., S. Wang, and D. Kim (2014), Moist static energy budget of the mjo during dynamo, *J. Atmos. Sci.*, *71*(11), 4276–4291.
Sobel, A. H., J. Nilsson, and L. M. Polvani (2001), The weak temperature gradient approximation and balanced tropical moisture waves*, *J. Atmos. Sci.*, *58*(23), 3650–3665.
Sooraj, K., D. Kim, J.-S. Kug, S.-W. Yeh, F.-F. Jin, and I.-S. Kang (2009), Effects of the low-frequency zonal wind variation on the high frequency atmospheric variability over the tropics, *Clim. Dyn.*, *33*(4), 495–507.
Stan, C., M. Khairoutdinov, C. A. DeMott, V. Krishnamurthy, D. M. Straus, D. A. Randall, J. L. Kinter, and J. Shukla (2010), An ocean-atmosphere climate simulation with an embedded cloud resolving model, *Geophys. Res. Lett.*, *37*, L01702, doi:10.1029/2009GL040822.
Subramanian, A. C., and G. J. Zhang (2014), Diagnosing MJO hindcast biases in NCAR cam3 using nudging during the dynamo field campaign, *J. Geophys. Res. Atmos.*, *119*, 7231–7253, doi:10.1002/2013JD021370.
Sugiyama, M. (2009a), The moisture mode in the quasi-equilibrium tropical circulation model. Part i: Analysis based on the weak temperature gradient approximation, *J. Atmos. Sci.*, *66*(6), 1507–1523.
Sugiyama, M. (2009b), The moisture mode in the quasi-equilibrium tropical circulation model. Part ii: Nonlinear behavior on an equatorial β plane, *J. Atmos. Sci.*, *66*(6), 1525–1542.
Taylor, K. E., R. J. Stouffer, and G. A. Meehl (2012), An overview of cmip5 and the experiment design, *Bull. Am. Meteorol. Soc.*, *93*(4), 485–498.
Trenberth, K. E. (1997), The definition of el nino, *Bull. Am. Meteorol. Soc.*, *78*(12), 2771–2777.
Ulate, M., C. Zhang, and J. Dudhia (2015), Role of water vapor and convection-circulation decoupling in mjo simulations by a tropical channel model, *J. Adv. Model. Earth Syst.*, *7*, 692–711, doi:10.1002/2014MS000393.
Waliser, D. E., K. Lau, and J.-H. Kim (1999), The influence of coupled sea surface temperatures on the Madden-Julian oscillation: A model perturbation experiment, *J. Atmos. Sci.*, *56*(3), 333–358.
Waliser, D. E., R. Murtugudde, and L. E. Lucas (2003), Indo-pacific ocean response to atmospheric intraseasonal variability: 1. Austral summer and the Madden-Julian oscillation, *J. Geophys. Res.*, *108*(C5), 3160, doi:10.1029/2002JC001620.
Wang, B., and X. Xie (1996), Low-frequency equatorial waves in vertically sheared zonal flow. Part i: Stable waves, *J. Atmos. Sci.*, *53*(3), 449–467.
Webster, P. J., A. M. Moore, J. P. Loschnigg, and R. R. Leben (1999), Coupled ocean–atmosphere dynamics in the indian ocean during 1997–98, *Nature*, *401*(6751), 356–360.
Werner, A., A. M. Maharaj, and N. J. Holbrook (2012), A new method for extracting the enso-independent Indian ocean dipole: Application to Australian region tropical cyclone counts, *Clim. Dyn.*, *38*(11–12), 2503–2511.
Wilson, E. A., A. L. Gordon, and D. Kim (2013), Observations of the Madden Julian oscillation during indian ocean dipole events, *J. Geophys. Res. Atmos.*, *118*, 2588–2599, doi:10.1002/jgrd.50241.
Yoneyama, K., et al. (2008), Mismo field experiment in the equatorial indian ocean*, *Bull. Am. Meteorol. Soc.*, *89*(12), 1889–1903.

Yu, J.-Y., and J. D. Neelin (1994), Modes of tropical variability under convective adjustment and the Madden-Julian oscillation. Part ii: Numerical results, *J. Atmos. Sci.*, *51*(13), 1895–1914.

Zhang, C., and M. Dong (2004), Seasonality in the Madden-Julian oscillation, *J. Clim.*, *17*(16), 3169–3180.

Zhang, C., and J. Gottschalck (2002), Sst anomalies of enso and the Madden-Julian oscillation in the equatorial pacific*, *J. Clim.*, *15*(17), 2429–2445.

Zhang, C., and H. H. Hendon (1997), Propagating and standing components of the intraseasonal oscillation in tropical convection, *J. Atmos. Sci.*, *54*(6), 741–752.

Zhang, C., M. Dong, S. Gualdi, H. H. Hendon, E. D. Maloney, A. Marshall, K. R. Sperber, and W. Wang (2006), Simulations of the Madden–Julian oscillation in four pairs of coupled and uncoupled global models, *Clim. Dyn.*, *27*(6), 573–592.

Zhao, Y., and S. Nigam (2015), The indian ocean dipole: A monopole in sst, *J. Clim.*, *28*(1), 3–19.